Phloretin enhances remyelination by stimulating oligodendrocyte precursor cell differentiation

Tess Dierckx[a], Sam Vanherle[a], Mansour Haidar[a], Elien Grajchen[a], Fleur Mingneau[a], Pascal Gervois[b], Esther Wolfs[b], Dany Bylemans[c,d], Arnout Voet[e], Tien Nguyen, Ibrahim Hamad[a,f], Markus Kleinewietfeld[a,f], Jeroen F. J. Bogie[a], and Jerome J. A. Hendriks[a,1]

Failure of remyelination underlies the progressive nature of demyelinating diseases such as multiple sclerosis. Why endogenous repair mechanisms frequently fail in these disorders is poorly understood. However, there is now evidence indicating that this is related to an overly inflammatory microenvironment combined with the intrinsic inability of oligodendrocyte precursor cells (OPCs) to differentiate into mature myelinating cells. Previously, we found that phloretin, a flavonoid abundantly present in apples and strawberries, reduces neuroinflammation by driving macrophages toward an antiinflammatory phenotype. Here, we show that phloretin also markedly stimulates remyelination in ex vivo and in vivo animal models. Improved remyelination was attributed to a direct impact of phloretin on OPC maturation and occurred independently from alterations in microglia function and inflammation. We found, mechanistically, that phloretin acts as a direct ligand for the fatty acid sensing nuclear receptor peroxisome proliferator-activated receptor gamma, thereby promoting the maturation of OPCs. Together, our findings indicate that phloretin has proregenerative properties in central nervous system disorders, with potentially broad implications for the development of therapeutic strategies and dietary interventions aimed at promoting remyelination.

multiple sclerosis | oligodendrocyte | phloretin | remyelination

Accumulation of disability in neurological disorders such as multiple sclerosis (MS) reflects an increasing burden of axonal injury and loss caused by repeated episodes of inflammatory demyelination (1, 2). Early in the course of MS, this neuroinflammatory response not only induces demyelination but also activates endogenous repair mechanisms that mediate the restoration of damaged myelin sheaths, a process called remyelination. Remyelination is carried out by oligodendrocytes and is characterized by distinct stages. First, expansion and mobilization of oligodendrocyte progenitor cells (OPCs) within the lesion area occur, followed by OPC differentiation into mature myelinating oligodendrocytes and remyelination of the affected axons (3–5). However, in progressive MS patients, remyelination frequently fails, resulting in chronically demyelinated plaques and gliotic scar tissue. This has profound pathophysiological consequences because loss of myelin not only disrupts axonal function but also compromises axon physical integrity by increasing susceptibility to inflammatory mediators and disrupting trophic support provided by myelinating oligodendrocytes (6–9). The exact reason why remyelination is hampered in these disorders is poorly understood. However, emerging evidence indicates that this is related to an overly inflammatory microenvironment in combination with the intrinsic inability of OPCs to differentiate into mature myelinating oligodendrocytes (10, 11). Therefore, current strategies to enhance remyelination involve approaches aimed at stimulating local central nervous system (CNS)–resident microglia and peripherally derived infiltrated macrophages toward a phenotype with antiinflammatory and reparative features (12–14). Another promising strategy to enhance repair is by directly manipulating signaling pathways that regulate OPC differentiation such as leucine rich repeat and immunoglobin-like domain-containing protein 1, Notch, wingless-related integration site (Wnt), and the peroxisome proliferator-activated receptor gamma (PPARγ) pathway (10, 13, 15, 16). Overall, therapeutics that influence both immune and repair processes are expected to be most efficient to promote remyelination.

Previously, we demonstrated that phloretin, a dihydrochalcone highly present in strawberries and apples and known to obtain immunomodulatory and antioxidative features, is able to alleviate neuroinflammation by altering the phenotype of phagocytes (17). In this study, we show that phloretin accelerates remyelination after cuprizone-induced demyelination as well. By using in vitro OPC cultures and microglia-depleted ex vivo brain slices, enhanced remyelination was found to be the result of a direct impact of phloretin on OPC maturation. Molecular docking and functional PPARγ antagonist/agonist experiments further illustrated that phloretin stimulates OPC differentiation by acting as a

Significance

The progressive nature of brain disorders such as multiple sclerosis (MS) reflects an increasing burden of axonal injury and loss induced by neuroinflammation and demyelination. Previously, we found that phloretin, a flavonoid abundantly present in apples and strawberries, reduces neuroinflammation by driving phagocytes toward an antiinflammatory phenotype. In this study, we provide evidence that phloretin enhances remyelination in ex vivo and in vivo animal models by stimulating oligodendrocyte precursor cell maturation. These results offer future perspectives for phloretin as a therapeutic strategy for neurodegenerative disorders such as MS.

potent PPARγ agonist. Because phloretin affects both the immunomodulatory and neurodegenerative aspects of MS, it holds potential as a natural treatment of this demyelinating disorder.

Materials and Methods

Antibodies and Chemical Reagents. Phloretin (Sigma-Aldrich) was dissolved in 50 mM KOH to a 15-mM stock solution and stored at −20 °C. Phloretin was administered daily at a concentration of 10 and 50 μM for in vitro and ex vivo experiments, respectively. For in vivo treatment, phloretin was dissolved in 1 N NaOH (pH was readjusted to 7.2 with 1 N HCL) and further diluted in physiological water to obtain a concentration of 50 mg/kg. GW9662 (10 nM; M6191, Sigma-Aldrich) and rosiglitazone (1 μM; R2408, Sigma-Aldrich) were used to inhibit or activate PPARγ, respectively. WY14643 (25 μM; C7081, Sigma-Aldrich) and GW501516 (0.1 μM; 43732, Sigma-Aldrich) were used to activate PPARα and PPARβ/γ, respectively. 7-Aminoactinomycin D (7AAD; 0.5 μg/mL; A1310, Thermo Fisher Scientific) was used to evaluate cellular viability. The following antibodies were used for immunofluorescence: rat anti–myelin basic protein (MBP; 1/500; MAB386, Millipore; brain cryosections and in vitro OPC cultures), rabbit anti–neurofilament (1/1,000; Ab8135, Abcam), rat anti-MBP (1/250; MCA409S, Millipore; cerebellar brain slices), mouse anti-O4 (1/1,000; MAB1326, R&D Systems), mouse anti-CC1 (1/50; ab16794, Abcam), and goat anti-olig2 (1/50; AF2418, R&D Systems). Appropriate secondary antibodies were purchased from Invitrogen.

Mice. Wild-type (WT) C57BL/6JOlaHsd mice (Envigo) were fed a regular diet and housed in the animal facility of the Biomedical Research Institute of Hasselt University. All experiments were performed according to institutional guidelines and were approved by the ethical committee for animal experiments of Hasselt University.

Cell Lines. Cos7/Oli-neu cells were cultured for the ligand-binding luciferase reporter assay in DMEM6429 (Sigma-Aldrich), supplemented with 1% penicillin/streptomycin (P/S; Invitrogen), 10% fetal calf serum (FCS; Invitrogen), and 1% L-glutamine (Sigma-Aldrich).

Bone Marrow–Derived Macrophages. Bone marrow–derived macrophages (BMDMs) were isolated from WT mice. BMDMs were obtained as described previously (18). In short, tibial and femoral bone marrow cells from 12-wk-old female WT mice were cultured in 10 cm Petri plates at a concentration of 10×10^6 cells/plate in RPMI1640 medium (Thermo Fisher Scientific) supplemented with 10% FCS, 1% P/S, and 15% L929-conditioned medium (LCM). After differentiation, BMDMs were detached at 37 °C with 10 mM EDTA in phosphate-buffered saline (PBS; Gibco) and cultured (0.5×10^6 cells/mL) in RPMI1640 supplemented with 10% FCS, 1%P/S, and 5% LCM at 37 °C and 5% CO_2.

OPC Isolation and Culturing. OPCs were isolated from pooled P0-P2 C57BL/6JOlaHsd neonatal mice cerebral cortices. Cortices were isolated, and meninges were removed, minced, and dissociated for 20 min at 37 °C with papain and DNase I (both 20 μg/mL; Sigma-Aldrich). The resulting mixed glial cultures were seeded in poly-L-lysine (PLL; 50 μg/mL; Sigma-Aldrich)–coated T75 flasks and cultured (37 °C; 8.5% CO_2) in DMEM6429 (Sigma-Aldrich) supplemented with 10% FCS and 1% P/S. After day 7, the medium was supplemented with insulin (5 μg/mL; Sigma-Aldrich). Medium changes were performed on days 4, 7, 11, and 14. Mixed glial cultures were separated after 14 d by mechanical shaking at 75 rpm for 45 min at 37 °C (to remove microglia) followed by additional 18-h shaking at 250 rpm at 37 °C. Medium containing the detached cells was then transferred to Petri dishes to further remove microglia and astrocytes based on differential adhesion characteristics (20 min; 37 °C; 8.5% CO_2). Afterward, the enriched OPCs were collected and plated in PLL-coated wells. OPCs were cultured in sato medium (DMEM; 100 μg/mL apo-transferrin, 16 μg/mL Putrescine, 5 μg/mL insulin, 60 ng/mL progesterone, 40 ng/mL sodium selenite, 30 ng/mL triiodothyronine, 40 ng/mL L-thyroxine, 1% P/S, 2% horse serum, and 2% B-27; all from Sigma-Aldrich) supplemented with platelet-derived growth factor (PDGF) and basic fibroblast growth factor (bFGF; both 10 μg/mL; Peprotech) for the first 2 days to reset their cell cycle. Afterward, OPCs were cultured in normal sato medium, and medium was changed every 2 days. Treatments were administered every day (phloretin 10 μM, GW9662 10 nM).

Ligand-Binding Luciferase Reporter Assay. To determine the activation of PPARγ, PPARα, and PPARβ/δ, ligand-binding luciferase reporter assays were performed using the ONE-GloTM Luciferase Assay System Kit (Promega). Cos7 or Oli-neu cells were transfected with bacterial plasmid constructs expressing luciferase under the control of the ligand-binding domain (LBD) for PPARγ, PPARα, or PPARβ/δ, which were provided by Bart Staels (National Institute of Health and Medical Research, University of Lille, Lille, France). Cells were grown to 60% confluency in 60-mm plates and transfected with 1.8 μg plasmid DNA including 0.2 μg pGAL4hPPARγ, pGAL4hPPARα, or pGAL4hPPARβ/δ, 1 μg pG5-TK-GL3, and 0.6 μg pCMV-β-galactosidase. JetPEI (Polyplus Transfection SA) was used as transfection reagent. Transfected cells were treated with vehicle, phloretin, or rosiglitazone for 1, 3, 6, or 18 h. Following treatment, cells were lysed in lysis buffer (25 mM glycyl-glycine, 15 mM $MgSO_4$, 4 mM EGTA, and 1× Triton; all from Sigma-Aldrich). To correct for transfection efficacy, β-galactosidase activity was measured using cell lysate (10%) in β-galactosidase buffer, consisting of 20% 2-nitrophenyl β-D-galactopyranoside (Sigma-Aldrich) and 80% Buffer-Z (0.1 M Na_2HPO_4, 10 mM KCl, 1 mM $MgSO_4$, and 3.4 μL/mL 2-mercaptoethanol; all Sigma-Aldrich). Luminescence and absorbance (410 nm) were measured using the FLUOstar Optima (BMG Labtech).

qPCR. Cell lysis was performed by using Qiazol Lysis reagent (Qiagen). RNA was extracted using the RNeasy Mini Kit (Qiagen). RNA concentration and quality were determined with a Nanodrop spectrophotometer (Isogen Life Science). Complementary DNA (cDNA) synthesis was performed by using the Quanta qScript cDNA SuperMix (Quanta Biosciences) per manufacturer instructions. qPCR was conducted on the StepOnePlus Real-Time PCR System (Applied Biosystems) using a SYBR green mix containing 1× SYBR green (Applied Biosystems), 0.3 μM primers (Integrated DNA Technologies), 12.5 ng cDNA, and nuclease-free water. The comparative Ct method was used to quantify gene expression. Data were normalized to the most stable reference genes cyclin A and hypoxanthine phosphoribosyltransferase 1. Primer sequences are available in *SI Appendix*, Table S1.

Viability Assay. BMDMs were treated with clodronate or empty liposomes (0.5 mg/mL; LIPOSOMA) for 24 h and washed, and medium was changed. Cellular viability was measured 7 d later by 7AAD according to manufacturer instructions (A1310, Thermo Fisher Scientific). OPCs were isolated and cultured for 2 d in PDGF- and bFGF-supplemented sato medium (also see *OPC Isolation and Culturing*), pretreated with vehicle or phloretin for 2 h, and treated with IFNγ/IL-1β (100 ng/mL; Peprotech). Cellular viability was measured 24 h later. The FACSCalibur was used to quantify cellular fluorescence.

Immunofluorescence and Analysis. Frozen brain cryosections were air dried and fixed in ice-cold acetone for 10 min at −20 °C. Cerebellar brain slices were fixed in 4% paraformaldehyde (PFA) for 15 min at room temperature (RT). Mouse OPCs were cultured on PLL-coated glass cover slides and fixed in 4% PFA for 30 min. Brain sections, cerebellar slices, and OPCs were blocked by using either Dako protein block (Agilent; 30 min), blocking buffer containing 5% horse serum and 0.3% Triton X-100 in PBS (1 h), or blocking buffer containing 1% BSA in 0.1% PBS-Tween (30 min), respectively. Afterward, they were incubated overnight at 4 °C with primary antibodies, washed, and incubated with the appropriate secondary antibodies for 1 h at RT. Images of brain cryosections and OPCs were taken using a Nikon Eclipse 80i microscope (10× objective) and NIS Elements BR 3.10 software (Nikon). To quantify the level of OPC maturation in vitro, MBP/O4 ratios per cell and Sholl analysis parameters related to process complexity and branching (sum intersections and average intersections per Sholl ring) were used as readouts. Sholl analysis was performed as described previously (19). Images of cerebellar brain slices were made on the LSM880 confocal microscope (Zeiss). The level of remyelination in brain slice was represented by the myelinating index, which was calculated by dividing the colocalized area of MBP and neurofilament (NF) by the total NF area. Colocalization was calculated using the colocalize threshold plugin in ImageJ. Three-dimensional rendering of cerebellar brain slices was done using vaa3d software (20). The images shown in the figures are digitally enhanced.

Molecular Docking. The structures of phloretin and rosiglitazone were taken from Protein Data Bank (PDB 2uxi) and further optimized in MOE v.2020 to find the dominant protomer (*SI Appendix*, Fig. S4 *D* and *E*) (21). Crystal structures of

PPARγ [PDB 2g0h (22), 2q5p (23), 2zk3 (24), 3b3k (25), 3cds (25), 3d6d (25), 3k8s (26, 27), 2zk1 (24), 5ycp (27)], PPARα [PDB 2p54 (28)], and PPARβ/δ [PDB 3tkm (29)] were prepared using the MOE QuickPrep function. Phloretin was docked into the LBD of the PPAR structures using the GOLD v.2020 Ensemble docking function (30).

Transmission Electron Microscopy. Brain samples were isolated and fixed with 2% glutaraldehyde. Afterward, the samples were postfixed in 2% osmium-tetroxide in 0.05 M sodium cacodylate buffer for 1 h at 4 °C. Samples were dehydrated by ascending concentrations of acetone and impregnated overnight in a 1:1 mixture of acetone and araldite epoxy resin. Thereafter, the samples were embedded in araldite epoxy resin at 60 °C, cut into slices of 70 nm (perpendicular to the corpus callosum [CC]; Leica EM UC6 microtome), and transferred to 0.7% formvar–coated copper grids (Aurion). The samples were contrasted with 0.5% uranyl acetate and lead citrate using a Leica EM AC20. Analysis was performed by using the Philips EM208 S electron microscope (Philips) equipped with a Morada Soft Imaging System camera with iTEM-FEI software (Olympus SIS). ImageJ was used to calculate the g-ratio (the ratio of the inner axonal diameter to the total outer diameter), using between four and eight images per animal.

Cerebellar Slice Cultures. Cerebellar slices were obtained from C57BL/6JOlaHsd mouse pups at the age of P9 or P10, as described previously (31, 32). To induce demyelination, slices were treated with lysolecithin (LPC; 0.5 mg/mL; Sigma-Aldrich) 3 d after isolation for 16 h. After demyelination, slices were treated daily with phloretin (50 μM) or vehicle for 6 d. For microglia depletion, slices were treated with clodronate or empty liposomes (0.5 mg/mL; LIPOSOMA) immediately after isolation for 24 h. After 3 d, slices were treated with LPC for 16 h followed by daily treatment with phloretin or vehicle.

Measurements of Nitric Oxide. Nitric oxide (NO) was indirectly monitored in the medium of the cerebellar brain slice cultures (BSCs) after 6 d of vehicle or phloretin treatment using the Griess Reagent Nitrite Measurement Kit (Abcam). Briefly, nitrite reacts with sulfanilamide and N-(1-naphthyl)ethylenediamine dihydrochloride to produce a pink azo dye. Absorbance of this azo derivative was then measured at 540 nM using a microplate reader (iMark, Bio-Rad).

In Vivo Cuprizone-Induced Demyelination. To induce demyelination, 10-wk-old male mice (n = 3–6) were fed ad libitum a diet of 0.3% cuprizone (bis[cyclohexanone]oxaldihydrazone; Sigma-Aldrich) mixed in powdered standard chow for 6 wk (6w). Mice were intraperitoneally injected daily with vehicle or phloretin (50 mg/kg) starting from the first day of cuprizone diet. Upon withdrawal of the cuprizone diet (6w), spontaneous remyelination occurred. Tissue was collected at 6w and after 1 wk of recovery (6 + 1w).

Statistical Analysis. GraphPad Prism was used to statistically analyze the data, which are represented as mean ± SEM. D'Agostino and Pearson omnibus normality test was used to test for normal distribution. Two-tailed unpaired Student t test (with Welch correction if necessary) was used for normally distributed data. Mann-Whitney analysis was used for data that did not pass the normality test. P values <0.05 were considered to demonstrate significant differences (*P < 0.05, **P < 0.01, ***P < 0.001, and ****P < 0.0001).

Results

Phloretin Promotes Repair after Cuprizone-Induced Demyelination.
To determine the impact of phloretin on remyelination, the cuprizone-induced de- and remyelination model was used. Cuprizone feeding results in toxic demyelination of diverse brain regions such as the CC, and switching to normal chow leads to spontaneous remyelination. After 6 wk of cuprizone feeding (6w), demyelination was observed in both vehicle- and phloretin-treated mice, as determined by transmission electron microscopy (TEM) and MBP staining analysis of the CC (Fig. 1 A–C). One week after cessation of cuprizone feeding (6 + 1w), phloretin-treated mice showed increased MBP protein levels (Fig. 1 A and B), increased CC1^{+} cells (SI Appendix, Fig. S1 A and B), and lower G ratios in the CC compared with

vehicle-treated mice, illustrating that phloretin enhanced remyelination. Furthermore, small-diameter axons showed thicker myelin sheaths in phloretin-treated mice compared with in control mice (Fig. 1D). In support of these findings, phloretin-treated animals displayed increased messenger RNA (mRNA) expression of Mbp and Plp, both after demyelination (6w) and during remyelination (6 + 1w) (Fig. 1 E and F). Surprisingly, no significant differences in number of phagocytes (F4/80^{+} cells) or gene expression levels of proinflammatory mediators (Ccl5, Nos2, Ccl4, Il6, Il1β, Tnfα) were observed between vehicle- and phloretin- treated mice at 6w and 6 + 1w (Fig. 1 G–J). Additionally, no differences were observed in the expression of the neurotrophic factors (Tgfβ, Cntf, Ngf, Igf1) or antioxidative genes, which we previously found to be up-regulated by phloretin and drive phagocytes toward a less-inflammatory phenotype (17), between vehicle- and phloretin-treated mice (SI Appendix, Fig. S1 C and D). We show that phloretin enhances remyelination after cuprizone-induced demyelination without significantly affecting the local inflammatory response.

Phloretin Stimulates OPC Maturation In Vitro.
Having established that phloretin stimulates remyelination without modulating the expression of inflammatory mediators, we next sought to determine whether phloretin enhances the intrinsic differentiation capacity of OPCs. For this purpose, OPC cultures were exposed to a differentiation mixture in the presence or absence of phloretin. Our data indicate that phloretin-treated OPCs show enhanced differentiation compared with vehicle-treated OPCs, evidenced by elevated mRNA levels of the mature oligodendrocyte markers Mbp and Plp and increased ratio of MBP over the preoligodendrocyte marker O4 (Fig. 2 A–C and SI Appendix, Fig. S2A). To confirm increased differentiation of OPCs upon phloretin treatment at a morphological level, Sholl analysis was performed. Sholl analysis demonstrated that phloretin-stimulated OPCs are characterized by an increased number of branches and a more complex branch geometry, morphological characteristics typically associated with more mature oligodendrocytes (Fig. 2 D and E). No effect of phloretin on oligodendrocyte viability was found (SI Appendix, Fig. S2B). Overall, these findings demonstrate that phloretin enhances OPC differentiation in vitro.

Phloretin Directly Enhances OPC Differentiation in Ex Vivo Brain Slices.
Previously, we showed that phloretin reduces neuroinflammation by driving macrophages toward an antiinflammatory phenotype. To determine whether phloretin promotes remyelination independently of acting on phagocytes, we used ex vivo cerebellar brain slice cultures (BSCs) demyelinated with LPC and depleted of microglia. In agreement with our in vivo findings, phloretin-treated BSCs showed enhanced remyelination compared with vehicle-treated slices, as demonstrated by a higher myelination index (Fig. 3 A and B). Mirroring this, higher protein levels of the mature oligodendrocyte marker CC1 were found in BSCs treated with phloretin (Fig. 3 C and D). To elucidate the role of microglia in these effects, we used slices in which microglia were depleted by clodronate liposomes. Efficacy of microglia depletion was confirmed in primary phagocyte cultures and in the BSC model (SI Appendix, Fig. S4 A–C). No difference in the remyelination index was found between BSCs treated with empty liposomes and those left untreated, ruling out any nonspecific effects (SI Appendix, Fig. S3D). Consistent with previous studies, microglia depletion with clodronate liposomes reduced the overall remyelination capacity of BSCs (Fig. 3B and SI Appendix, Fig. S3E) (33, 34). Interestingly, in the absence of microglia, phloretin
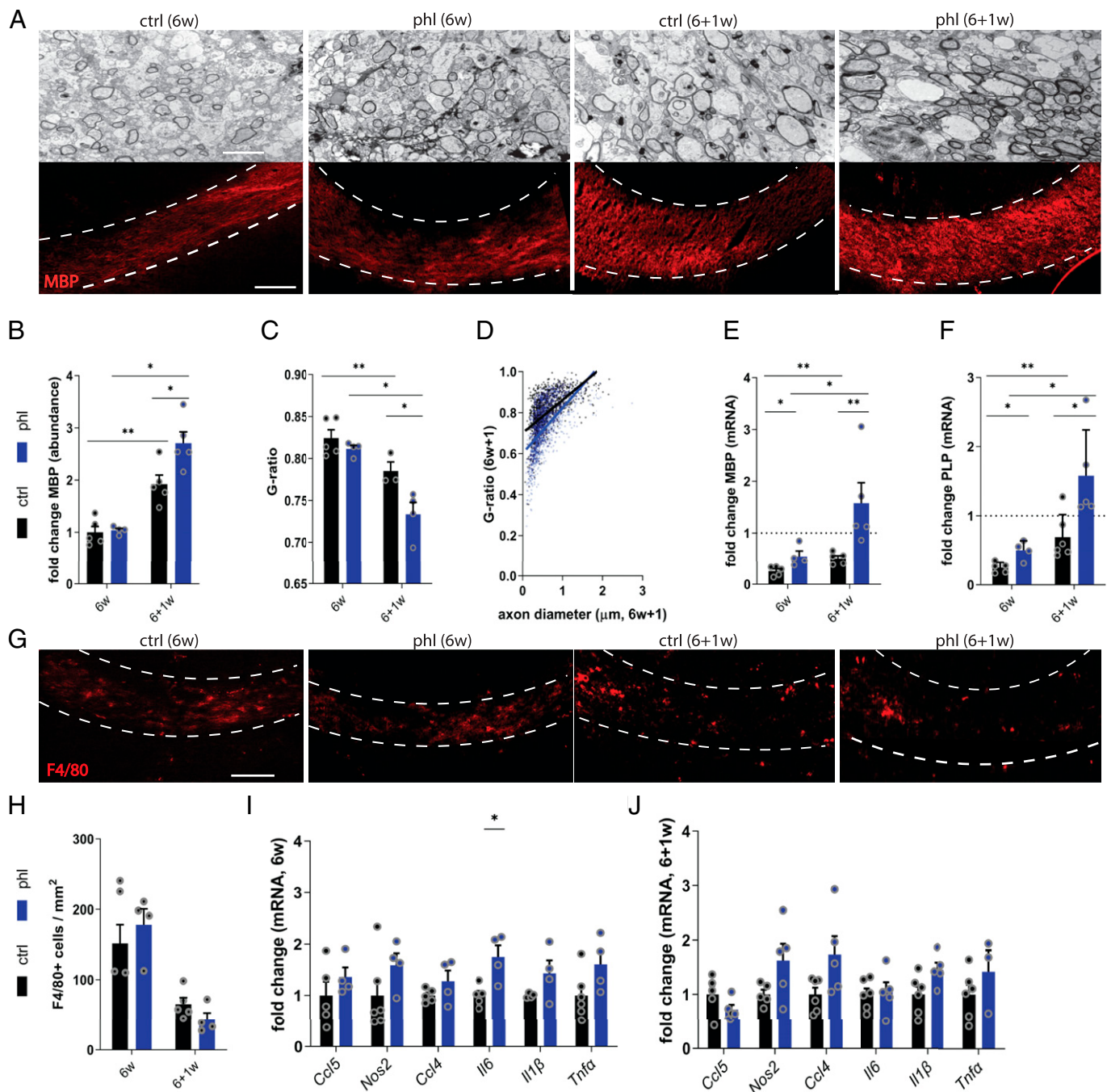
Fig. 1. Phloretin promotes repair after cuprizone-induced demyelination. (*A*) Representative images of TEM and immunofluorescence MBP staining analysis of CC from vehicle- or phloretin-treated mice (*n* = 3–6) after cuprizone-induced demyelination (6w) and subsequent remyelination (6 + 1w). The outer border of the CC is defined by a dotted line. Scale bars, 100 μm (MBP staining); 2 μm (TEM). (*B*) Remyelination efficacy (ratio of the amount of myelination at 6 + 1w over the amount of myelination at 6w using MBP staining) in CC from vehicle- or phloretin-treated mice. (*C* and *D*) Analysis of the g-ratio (ratio of the inner axonal diameter to the total outer diameter) and g-ratio in function of the axon diameter in CC from vehicle- or phloretin-treated mice. (*E* and *F*) mRNA expression of myelin proteins *Mbp* and *Plp* in the CC of vehicle- or phloretin-treated mice at 6w and 6 + 1w. Dotted line represents animals fed normal chow. (*G* and *H*) Representative immunofluorescence images and quantification of F4/80 staining in the CC from vehicle- or phloretin-treated mice at 6w and 6 + 1w. Scale bar, 100 μm. (*I* and *J*) mRNA expression of inflammatory mediators in the CC of vehicle- or phloretin-treated mice at 6w and 6 + 1w. Ctrl, control; phl, phloretin. Data are represented as mean ± SEM *$P < 0.05$ and **$P < 0.01$ (unpaired *t* test, two tailed).

was able to boost remyelination (50% increase) at a similar potency as in the brain slices that contained microglia (48% increase) (Fig. 3 *A* and *B*). In agreement with our findings in the cuprizone model, no significant differences in mRNA expression of *Ccl5*, *Ccl4*, *Il6*, *Il1β*, or *Nos2* or release of nitric oxide (NO) were found between vehicle- and phloretin-treated BSCs (Fig. 3 *E* and *F*). The abovementioned findings support the notion that phloretin promotes remyelination by inducing OPC differentiation independently of microglia modulation.

Phloretin Stimulates OPC Maturation in a PPARγ-Dependent Manner. Given that our previous RNA sequencing data demonstrated that phloretin activates PPAR signaling and that PPARγ plays an essential role in OPC differentiation, we next assessed whether phloretin stimulates OPC differentiation via PPARγ (17, 35, 36). By using ligand-binding luciferase reporter assays, we show that phloretin activates PPARγ in a dose-dependent manner, with an EC_{50} value of 11.61 μM (Fig. 4*A* and *SI Appendix*, Fig. S4*A*). Interestingly, phloretin did not activate the
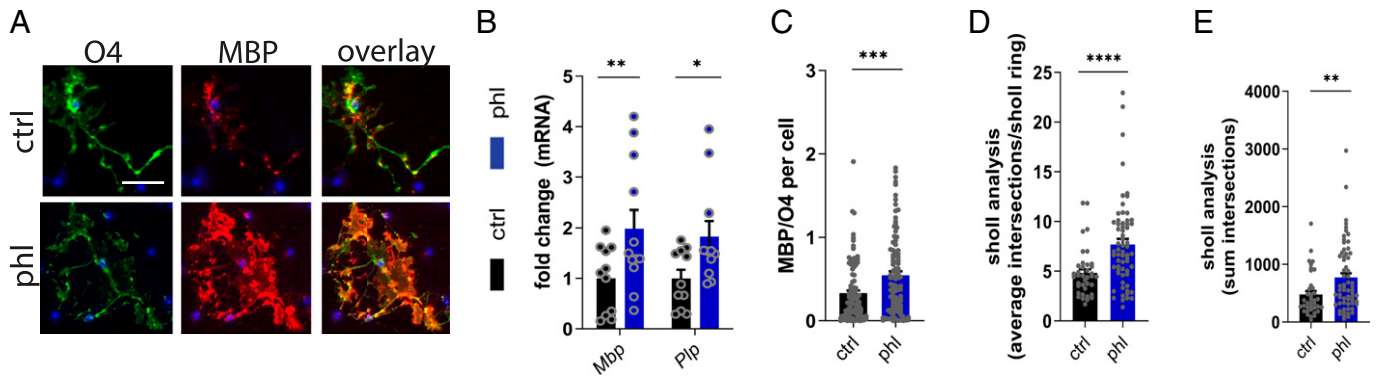
Fig. 2. Phloretin stimulates oligodendrocyte precursor cell maturation in vitro. (*A*) Representative immunofluorescence images of OPCs treated with vehicle or phloretin and stained for the premature oligodendrocyte marker O4 and the mature oligodendrocyte marker MBP. Scale bar, 25 μm. (*B*) mRNA levels of myelin proteins *Mbp* and *Plp* in vehicle- or phloretin-treated OPCs (n = 10–11 wells; three independent experiments) (*C*) Quantification of the MBP/O4 staining represented as the ratio of MPB over O4 per cell in OPCs treated with vehicle or phloretin (n = 100+ cells; two independent experiments). (*D–E*) Sholl analysis (related to process complexity and branching of OPCs) of OPCs treated with vehicle or phloretin as a readout parameter for OPC differentiation (n = 40+ cells; two independent experiments). Ctrl, control; phl, phloretin. Data are represented as mean ± SEM. *$P < 0.05$, **$P < 0.01$, ***$P < 0.001$, and ****$P < 0.0001$ (unpaired *t* test, two tailed).

other PPAR isoforms PPARα and PPARβ/δ (*SI Appendix*, Fig. S4 *B* and *C*). Time-dependent PPARγ luciferase reporter experiments further demonstrated rapid PPARγ activation upon phloretin treatment, comparable to rosiglitazone, suggesting that phloretin acts as a direct ligand for PPARγ (Fig. 4*B* and *SI Appendix,* Fig. S4 *D–F*). Accordingly, molecular docking analysis unraveled that phloretin obtains a ligand binding mode similar to that of other known PPARγ agonists and confirmed PPARγ isoform specificity, evidenced by a higher GoldScore docking affinity score (PPARγ, 74.7; PPARα, 61.6; and PPARβ/δ, 58.7) (Fig. 4*C* and *SI Appendix,* Fig. S4*G*). In support of these findings, phloretin-treated OPCs, BSCs, and cuprizone animals displayed increased expression of the PPARγ response genes *Cd36*, *ApoE*, *Abca1*, and *Cpta1* (Fig. 4 *D–G* and *SI Appendix,* Fig. S4 *H and I*). Next, to establish whether phloretin stimulates OPC differentiation via PPARγ, the PPARγ-specific antagonist GW9662 was used. The PPARγ antagonist reversed the increased *Mbp* and *Plp* expression, MBP/O4 ratio, and branch quantity and complexity following phloretin exposure (Fig. 4 *H–L*). Importantly, PPARγ antagonism counteracted the reparative impact of phloretin in BSCs (Fig. 4*M*). In the absence of phloretin, no effect of the PPARγ antagonist on in vitro OPC differentiation or ex vivo BSC remyelination was observed (Fig. 4 *N* and *O*). Collectively, these findings show that phloretin is a potent PPARγ agonist and thereby stimulates OPC maturation and remyelination.

Discussion

In this study, we show that phloretin stimulates CNS repair after cuprizone-induced demyelination by enhancing the intrinsic differentiation capacity of OPCs. Direct peroxisome PPARγ activation by phloretin was found to drive OPC maturation. Given the potent immunomodulatory properties of phloretin (17), our findings highlight the therapeutic promise of dietary phloretin to simultaneously reduce neuroinflammation and enhance CNS repair, potentially being of therapeutic interest in early and late disease stages of chronic inflammatory, neurodegenerative disorders such as MS.

Increasing evidence indicates that failure of remyelination is related to an inhibitory inflammatory microenvironment combined with the intrinsic inability of OPCs to mature into myelinating cells (10, 11). Our data indicate that phloretin induces remyelination in in vivo and ex vivo models by directly enhancing OPC maturation. Consistent with our findings, a number of studies have

demonstrated the potential of boosting OPC maturation as a strategy to stimulate remyelination (37–40). Intriguingly, while enhanced remyelination was established independently of phagocyte modulation, we recently demonstrated that phloretin lowers neuroinflammation in the experimental autoimmune encephalomyelitis (EAE) model by affecting the phenotype of infiltrated macrophages (17). Several factors may be responsible for the differential impact of phloretin on the neuroinflammatory burden in the EAE and the cuprizone models. First, the relative contribution of systemic immunity differs between both models. While EAE disease pathology relies predominantly on a systemic autoimmune response, the pathology in the cuprizone model is primarily driven by changes in the inflammatory properties of glial cells. Accordingly, the impact of phloretin in the EAE model was associated with reduced levels of blood-derived monocyte-derived macrophages in the CNS, and thus, the observed effects in this model may be partially due to prevention of immune cell infiltration by phloretin. Alternatively, because the EAE model is characterized by less substantial demyelination and abundance of foamy phagocytes compared with the cuprizone model, it is possible that phloretin exerts different effects in foamy phagocytes compared with phagocytes that do not contain myelin. Finally, the time point of analysis may play a role in the differential effects observed, because neuroinflammation in the EAE model was monitored in the acute disease stage, characterized by active immune cell infiltration, while the cuprizone model is characterized by chronic low-grade inflammation. This study demonstrates that phloretin, aside from lowering neuroinflammation in the EAE model, stimulates CNS repair without significantly affecting the inflammatory response in the cuprizone model.

Our results demonstrate that the nuclear receptor PPARγ drives phloretin-induced OPC maturation. In agreement with our findings, phloretin is reported to activate PPARγ signaling in adipocytes (35, 36). Moreover, the PPARγ pathway is known to stimulate OPC maturation (41–43). Mechanistically, the proregenerative impact of PPARγ is associated with changes in cellular lipid metabolism, oxidative stress regulation, and enhanced mitochondrial function (44). Interestingly, we previously found that phloretin activates the antioxidative nuclear factor-erythroid factor 2–related factor 2 pathway in macrophages (17). On this note, a more in-depth follow-up study investigating oxidative stress regulation, changes in lipid metabolism, and mitochondrial function in phloretin-stimulated OPC maturation would be of interest.
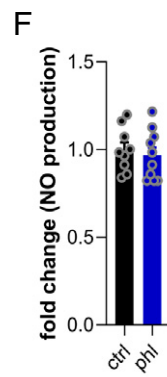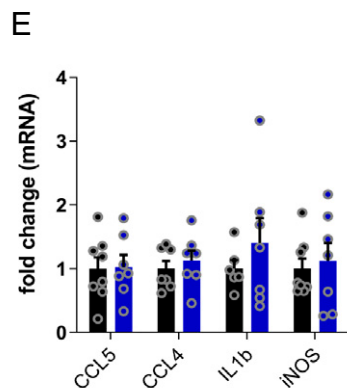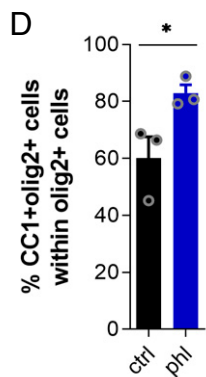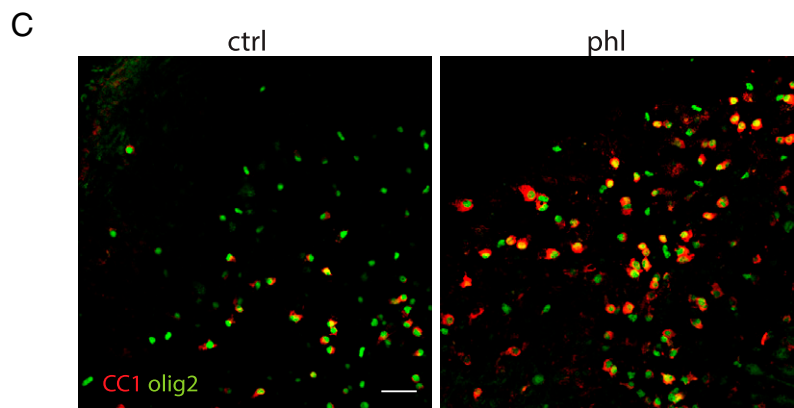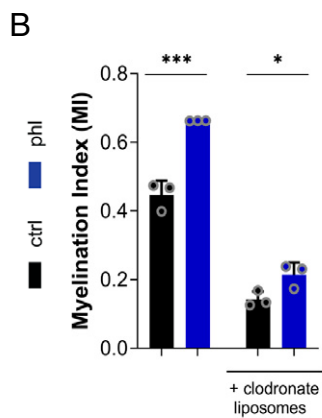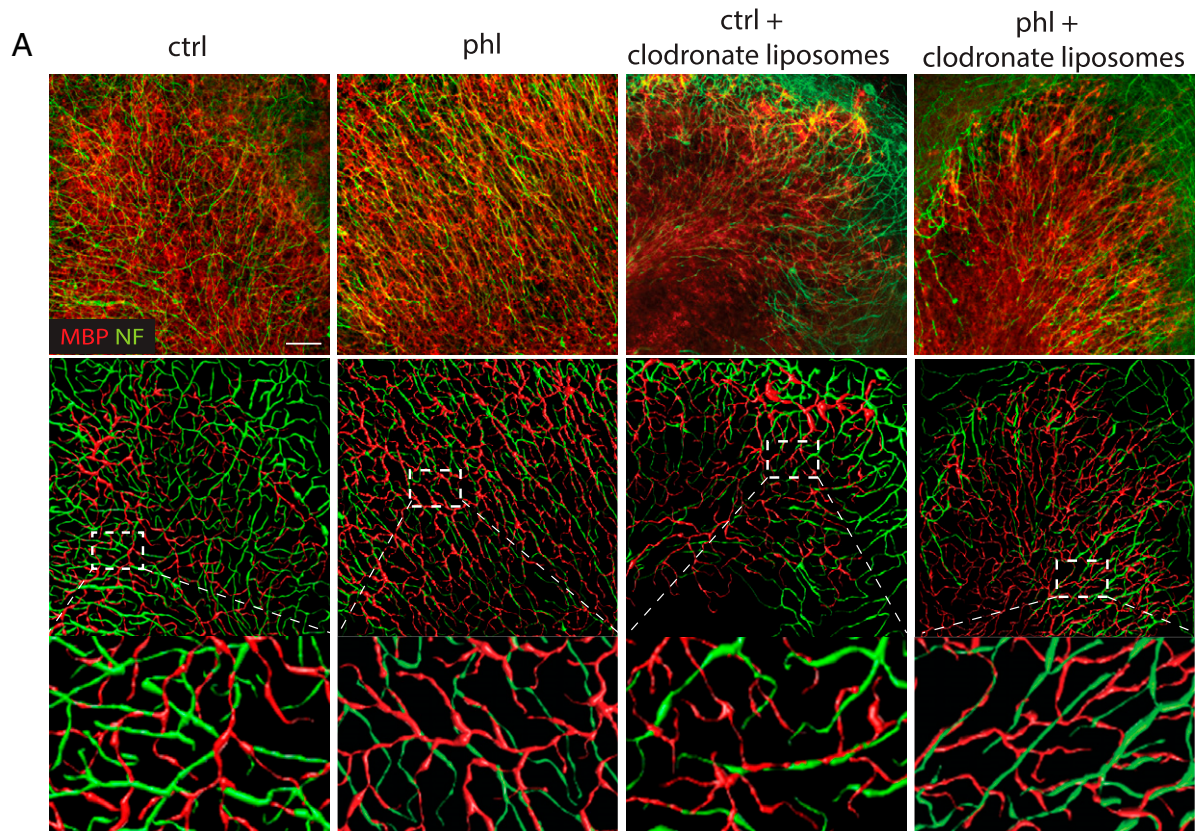
Fig. 3. Phloretin directly enhances OPC differentiation in ex vivo brain slices. (*A*) Representative immunofluorescence images and three-dimensional reconstructions of vehicle- or phloretin-treated BSCs stimulated with or without clodronate liposomes. Scale bar, 50 μm. (*B*) Myelination index of vehicle- or phloretin-stimulated BSCs stimulated with our without clodronate liposomes (*n* = 3). (*C* and *D*) Representative immunofluorescence images and quantification of vehicle- and phloretin-treated BSCs stained for the oligodendrocyte lineage marker olig2 and mature oligodendrocyte CC1 marker (*n* = 3). Scale bar, 50 μm. (*E* and *F*) mRNA levels of inflammatory mediators (*n* = 6–8) and NO production (*n* = 9–10) in BSC medium of vehicle- or phloretin-treated BSCs. Ctrl, control; phl, phloretin. Data are represented as mean ± SEM. *P < 0.05 and ***P < 0.001 (unpaired *t* test, two tailed).
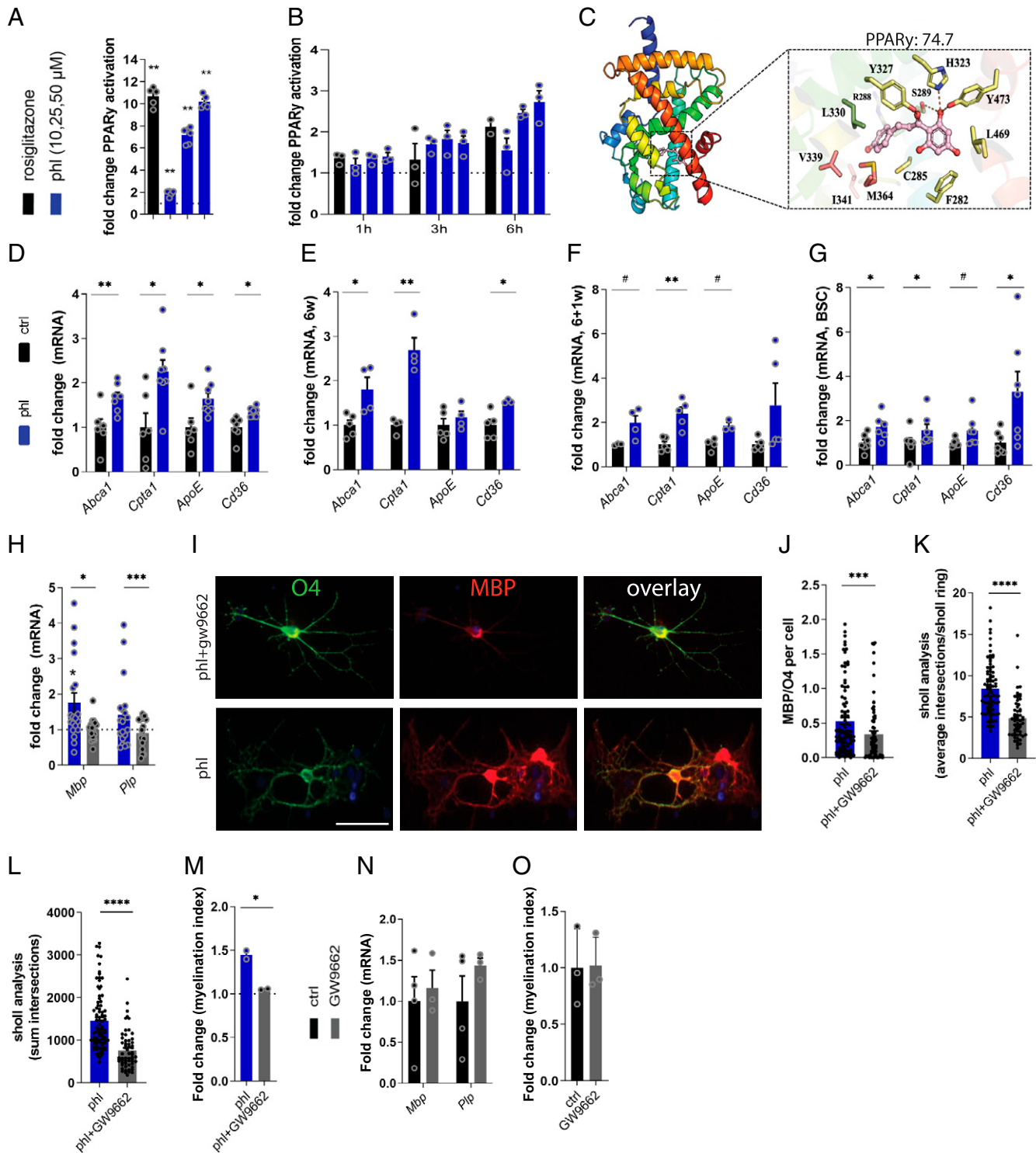
Fig. 4. Phloretin stimulates OPC maturation in a PPARγ-dependent manner. (*A*) Luciferase assay illustrating a dose–response activation of PPARγ in cos7 cells treated with the PPARγ agonist rosiglitazone (1 μM) or different phloretin concentrations (from Left to Right: 10, 25, and 50 μM) for 18 h (n = 5–6). (*B*) Luciferase assay illustrating a dose–response activation of PPARγ in Oli-neu cells after 1-, 3-, and 6-h rosiglitazone (1 μM) or phloretin treatment (from *Left* to *Right*: 10, 25, and 50 μM) (n = 2–3). (*C*) The PPARγ LBD consists of three arms (1, 2, and 3), which are shown in yellow, pink, and green sticks, respectively. Phloretin interacts with three arms of the PPARγ LBD: arm 1 residues Ser289, His323, Tyr473, and Tyr327 form hydrogen bonds with the protonated hydroxyl group and the middle carbonyl group of phoretin, arm 2 residues Val339, Ileu341, and Met364, and arm 3 residues Arg288 and Leu330 make hydrophobic interactions with the aromatic ring of phloretin. Phloretin obtained the highest docking score in the LBD of the PPARγ isoform (74,6913) (*D–G*) mRNA expression of PPARγ response genes in OPCs (n = 6–8; two independent experiments), cuprizone mice (6w and 6+1w; n = 3–5), and BSCs (n = 6–7) treated with vehicle or phloretin. (*H*) mRNA expression of myelin protein *Mbp* and *Plp* in OPCs treated with phloretin or phloretin and the PPARγ antagonist GW9662. Dotted line represents OPCs treated with vehicle (n = 12–14; three independent experiments). (*I* and *J*) Representative immunofluorescence images and quantification of MBP/O4 staining on OPCs treated with phloretin or phloretin and the PPARγ antagonist GW9662 (n = 70+ cells; two independent experiments). Scale bar, 25 μm. (*K* and *L*) Sholl analysis (related to process complexity and branching) of OPCs treated with phloretin or phloretin and PPARγ antagonist GW9662 as a readout parameter of OPC differentiation (n = 60+ cells; two independent experiments). (*M*) Myelination index of phloretin- and phloretin plus GW9662–treated BSCs (n = 2). (*N*) *Mbp* and *Plp* gene expression levels in control OPCs and OPCs treated with the PPARγ antagonist GW9662 (n = 3–4). (*O*) Myelinating index of control cerebellar BSCs and BSCs treated with the PPARγ antagonist GW9662 (n = 3). Ctrl, control; phl, phloretin. Data are represented as mean ± SEM. #P = 0.05, *P < 0.05, **P < 0.01, ***P < 0.001, and ****P < 0.0001 (unpaired t test, two tailed).

Our findings illustrate that phloretin acts as a direct agonist for PPARγ. Accordingly, the estimated binding affinity of phloretin to PPARγ is substantially higher than that to PPARα and PPARβ/δ. Generally, PPAR agonists can interact with three arms of the LBD. Arm 1 forms hydrogen bonds with the hydrophilic head groups of agonists and by doing so stabilizes the binding of coactivator proteins and activates gene transcription (45). Arms 2 and 3 exhibit further predominantly hydrophobic contacts with the hydrophobic tail of the PPAR agonist (Fig. 4C) (29, 45). The hydrogen bond between the middle carbonyl group of phloretin and the Tyr327 residue of the PPARγ LBD is not observed in PPARα or PPARβ/δ, because Tyr327 is not conserved in those isoforms and is replaced by Phe318 or Phe291, respectively. Taking this into account, the PPARγ specificity of phloretin is likely due to the stronger hydrogen bonding with arm 1 compared with PPARα and PPARβ/δ. An additional explanation may be the difference in hydrophobic contacts between phloretin and the PPAR LBDs. Specifically, while the tail of phloretin was orientated toward arm 2 in the PPARγ LBD, it was orientated toward arm 3 in the LBDs of PPARα and PPARβ/δ. Together, our findings demonstrate that phloretin is a potent PPARγ ligand and thereby promotes OPC maturation.

Natural substances are (re)emerging as promising therapeutic lead compounds in regenerative medicine, because they often have minimal adverse effects and can be superior in terms of biological and pharmacological activities as compared with synthetic compounds (46–48). Highlighting the latter, the potential of flavonoids to improve remyelination in MS patients was emphasized in a recent meta-analysis in which potentially remyelinating interventions in animal models of toxic demyelination were assessed (49). When we relate the phloretin concentrations used in this study to the consumption of apples, it corresponds to a daily intake of two to 10 apples in mice depending on the variety (50) and more than 1,000 kg apples in humans, which is not in the range of our normal dietary habits. Moreover, because phloretin was injected intraperitoneally in this study and the bioavailability of flavonoids after ingestion is generally low (51, 52), the number of apples needed to reach effective blood concentrations would even be higher. However, apples contain approximately 50 times more phloridzin, the glycosidic form of phloretin, which can be hydrolyzed to phloretin in the intestines (53), thereby being an important source of phloretin next to the aglycone itself. Moreover, apples contain other components such as ursolic acid that have been shown to reduce neuroinflammation and stimulate remyelination. Interestingly, similar to phloretin, ursolic acid was found to promote CNS repair in a PPARγ-dependent manner (54). Therefore, future studies should define if dietary apple consumption or phloretin/ursolic acid concentrated extracts can modulate MS disease processes in a similar manner as treatment with the standalone drug phloretin.

Our study shows that phloretin enhances remyelination by directly stimulating OPC maturation through activation of PPARγ. Phloretin has proregenerative properties in CNS disorders, with potentially broad implications for the development of therapeutic strategies and dietary interventions.

Author affiliations: [a]Department of Immunology and Infection, Biomedical Research Institute, Hasselt University, Diepenbeek 3590, Belgium; [b]Group of Cardio & Organ Systems, Biomedical Research Institute, Hasselt University, Diepenbeek 3590, Belgium; [c]Research Station for Fruit Cultivation, Sint-Truiden 3800, Belgium; [d]Department of Biosystems, Katholieke Universiteit Leuven, Heverlee 3001, Belgium; [e]Department of Chemistry, Laboratory for Biomolecular Modelling and Design, Katholieke Universiteit Leuven, Heverlee 3001, Belgium; and [f]Vlaams Instituut voor Biotechnologie (VIB) Laboratory of Translational Immunomodulation, VIB Center for Inflammation Research, Hasselt University, Diepenbeek 3590, Belgium

1. M. Filippi et al., Multiple sclerosis. Nat. Rev. Dis. Primers 4, 43 (2018).
2. E. C. Tallantyre et al., Clinico-pathological evidence that axonal loss underlies disability in progressive multiple sclerosis. Mult. Scler. 16, 406–411 (2010).
3. I. C. Di Bello, M. R. Dawson, J. M. Levine, R. Reynolds, Generation of oligodendroglial progenitors in acute inflammatory demyelinating lesions of the rat brain stem is associated with demyelination rather than inflammation. J. Neurocytol. 28, 365–381 (1999).
4. A. Sherafat, F. Pfeiffer, A. M. Reiss, W. M. Wood, A. Nishiyama, Microglial neuropilin-1 promotes oligodendrocyte expansion during development and remyelination by trans-activating platelet-derived growth factor receptor. Nat. Commun. 12, 2265 (2021).
5. M. Watanabe, Y. Toyama, A. Nishiyama, Differentiation of proliferated NG2-positive glial progenitor cells in a remyelinating lesion. J. Neurosci. Res. 69, 826–836 (2002).
6. J. Correale, M. I. Gaitán, M. C. Ysrraelit, M. P. Fiol, Progressive multiple sclerosis: From pathogenic mechanisms to treatment. Brain 140, 527–546 (2017).
7. J. Correale, M. F. Farez, The role of astrocytes in multiple sclerosis progression. Front. Neurol. 6, 180 (2015).
8. K. Hagemeier, W. Brück, T. Kuhlmann, Multiple sclerosis - Remyelination failure as a cause of disease progression. Histol. Histopathol. 27, 277–287 (2012).
9. K. A. Hanafy, J. A. Sloane, Regulation of remyelination in multiple sclerosis. FEBS Lett. 585, 3821–3828 (2011).
10. S. P. Fancy et al., Overcoming remyelination failure in multiple sclerosis and other myelin disorders. Exp. Neurol. 225, 18–23 (2010).
11. R. J. Franklin, Why does remyelination fail in multiple sclerosis? Nat. Rev. Neurosci. 3, 705–714 (2002).
12. J. F. J. Bogie et al., Stearoyl-CoA desaturase-1 impairs the reparative properties of macrophages and microglia in the brain. J. Exp. Med. 217, e20191660 (2020).
13. R. J. Franklin, C. Ffrench-Constant, Remyelination in the CNS: From biology to therapy. Nat. Rev. Neurosci. 9, 839–855 (2008).
14. E. Grajchen et al., CD36-mediated uptake of myelin debris by macrophages and microglia reduces neuroinflammation. J. Neuroinflammation 17, 224 (2020).
15. S. Mi et al., LINGO-1 negatively regulates myelination by oligodendrocytes. Nat. Neurosci. 8, 745–751 (2005).
16. R. A. Rudick, S. Mi, A. W. Sandrock Jr., LINGO-1 antagonists as therapy for multiple sclerosis: In vitro and in vivo evidence. Expert Opin. Biol. Ther. 8, 1561–1570 (2008).
17. T. Dierckx et al., Phloretin suppresses neuroinflammation by autophagy-mediated Nrf2 activation in macrophages. J. Neuroinflammation 18, 148 (2021).
18. J. F. Bogie et al., Scavenger receptor collectin placenta 1 is a novel receptor involved in the uptake of myelin by phagocytes. Sci. Rep. 7, 44794 (2017).
19. J. C. Murtie, W. B. Macklin, G. Corfas, Morphometric analysis of oligodendrocytes in the adult mouse frontal cortex. J. Neurosci. Res. 85, 2080–2086 (2007).
20. H. Peng, A. Bria, Z. Zhou, G. Iannello, F. Long, Extensible visualization and analysis for multidimensional images using Vaa3D. Nat. Protoc. 9, 193–208 (2014).
21. Molecular Operating Environment (MOE) CCGU, 1010 Sherbooke St. West, Suite #910, Montreal, QC, Canada, H3A 2R7, 2021.
22. I. L. Lu et al., Structure-based drug design of a novel family of PPARgamma partial agonists: Virtual screening, X-ray crystallography, and in vitro/in vivo biological activities. J. Med. Chem. 49, 2703–2712 (2006).
23. J. B. Bruning et al., Partial agonists activate PPARgamma using a helix 12 independent mechanism. Structure 15, 1258–1271 (2007).
24. T. Waku et al., Structural insight into PPARgamma activation through covalent modification with endogenous fatty acids. J. Mol. Biol. 385, 188–199 (2009).
25. R. Montanari et al., Crystal structure of the peroxisome proliferator-activated receptor gamma (PPARgamma) ligand binding domain complexed with a novel partial agonist: A new region of the hydrophobic pocket could be exploited for drug design. J. Med. Chem. 51, 7768–7776 (2008).
26. Y. Li et al., T2384, a novel antidiabetic agent with unique peroxisome proliferator-activated receptor gamma binding properties. J. Biol. Chem. 283, 9168–9176 (2008).
27. J. Y. Jang et al., Structural basis for the enhanced anti-diabetic efficacy of lobeglitazone on PPARγ. Sci. Rep. 8, 31 (2018).
28. M. L. Sierra et al., Substituted 2-[(4-aminomethyl)phenoxy]-2-methylpropionic acid PPARalpha agonists. 1. Discovery of a novel series of potent HDLc raising agents. J. Med. Chem. 50, 685–695 (2007).
29. F. A. Batista et al., Structural insights into human peroxisome proliferator activated receptor delta (PPAR-delta) selective ligand binding. PLoS One 7, e33643 (2012).
30. G. Jones, P. Willett, R. C. Glen, A. R. Leach, R. Taylor, Development and validation of a genetic algorithm for flexible docking. J. Mol. Biol. 267, 727–748 (1997).
31. R. Hussain et al., Progesterone and Nestorone facilitate axon remyelination: A role for progesterone receptors. Endocrinology 152, 3820–3831 (2011).
32. D. Meffre, C. Massaad, J. Grenier, Lithium chloride stimulates PLP and MBP expression in oligodendrocytes via Wnt/β-catenin and Akt/CREB pathways. Neuroscience 284, 962–971 (2015).
33. V. E. Miron et al., M2 microglia and macrophages drive oligodendrocyte differentiation during CNS remyelination. Nat. Neurosci. 16, 1211–1218 (2013).

34. M. R. Kotter, A. Setzu, F. J. Sim, N. Van Rooijen, R. J. Franklin, Macrophage depletion impairs oligodendrocyte remyelination following lysolecithin-induced demyelination. *Glia* **35**, 204–212 (2001).

35. G. Shu *et al.*, Phloretin promotes adipocyte differentiation in vitro and improves glucose homeostasis in vivo. *J. Nutr. Biochem.* **25**, 1296–1308 (2014).

36. M. Hassan *et al.*, Phloretin enhances adipocyte differentiation and adiponectin expression in 3T3-L1 cells. *Biochem. Biophys. Res. Commun.* **361**, 208–213 (2007).

37. F. Mei *et al.*, Accelerated remyelination during inflammatory demyelination prevents axonal loss and improves functional recovery. *eLife* **5**, 5 (2016).

38. R. R. Voskuhl *et al.*, Gene expression in oligodendrocytes during remyelination reveals cholesterol homeostasis as a therapeutic target in multiple sclerosis. *Proc. Natl. Acad. Sci. U.S.A.* **116**, 10130–10139 (2019).

39. F. J. Najm *et al.*, Drug-based modulation of endogenous stem cells promotes functional remyelination in vivo. *Nature* **522**, 216–220 (2015).

40. K. L. H. Cole, J. J. Early, D. A. Lyons, Drug discovery for remyelination and treatment of MS. *Glia* **65**, 1565–1589 (2017).

41. S. Kanakasabai *et al.*, PPARγ agonists promote oligodendrocyte differentiation of neural stem cells by modulating stemness and differentiation genes. *PLoS One* **7**, e50500 (2012).

42. W. N. Wan Ibrahim *et al.*, Perfluorooctane sulfonate induces neuronal and oligodendrocytic differentiation in neural stem cells and alters the expression of PPARγ in vitro and in vivo. *Toxicol. Appl. Pharmacol.* **269**, 51–60 (2013).

43. A. D. Roth *et al.*, PPAR gamma activators induce growth arrest and process extension in B12 oligodendrocyte-like cells and terminal differentiation of cultured oligodendrocytes. *J. Neurosci. Res.* **72**, 425–435 (2003).

44. W. Cai *et al.*, Peroxisome proliferator-activated receptor γ (PPARγ): A master gatekeeper in CNS injury and repair. *Prog. Neurobiol.* **163-164**, 27–58 (2018).

45. P. Markt, D. Schuster, J. Kirchmair, C. Laggner, T. Langer, Pharmacophore modeling and parallel screening for PPAR ligands. *J. Comput. Aided Mol. Des.* **21**, 575–590 (2007).

46. S. Schaffer, B. Halliwell, Do polyphenols enter the brain and does it matter? Some theoretical and practical considerations. *Genes Nutr.* **7**, 99–109 (2012).

47. T. B. Krasieva, J. Ehren, T. O'Sullivan, B. J. Tromberg, P. Maher, Cell and brain tissue imaging of the flavonoid fisetin using label-free two-photon microscopy. *Neurochem. Int.* **89**, 243–248 (2015).

48. D. Vauzour, Dietary polyphenols as modulators of brain functions: Biological actions and molecular mechanisms underpinning their beneficial effects. *Oxid. Med. Cell. Longev.* **2012**, 914273 (2012).

49. C. R. Hooijmans *et al.*, Remyelination promoting therapies in multiple sclerosis animal models: A systematic review and meta-analysis. *Sci. Rep.* **9**, 822 (2019).

50. D. Zielinska, J. M. Laparra-Llopis, H. Zielinski, D. Szawara-Nowak, J. A. Giménez-Bastida, Role of apple phytochemicals, phloretin and phloridzin, in modulating processes related to intestinal inflammation. *Nutrients* **11**, E1173 (2019).

51. A. Stalmach *et al.*, Absorption, metabolism, and excretion of green tea flavan-3-ols in humans with an ileostomy. *Mol. Nutr. Food Res.* **54**, 323–334 (2010).

52. U. Ullmann *et al.*, A single ascending dose study of epigallocatechin gallate in healthy volunteers. *J. Int. Med. Res.* **31**, 88–101 (2003).

53. P. Malathi, R. K. Crane, Phlorizin hydrolase: A beta-glucosidase of hamster intestinal brush border membrane. *Biochim. Biophys. Acta* **173**, 245–256 (1969).

54. Y. Zhang *et al.*, A dual effect of ursolic acid to the treatment of multiple sclerosis through both immunomodulation and direct remyelination. *Proc. Natl. Acad. Sci. U.S.A.* **117**, 9082–9093 (2020).